

The genomic landscape of response to EGFR blockade in colorectal cancer

Andrea Bertotti^{1,2,3*}, Eniko Papp^{4*}, Siân Jones⁵, Vilmos Adleff⁴, Valsamo Anagnostou⁴, Barbara Lupo^{1,2}, Mark Sausen⁵, Jillian Phallen⁴, Carolyn A. Hruban⁴, Collin Tokheim⁶, Noushin Niknafs⁶, Monica Nesselbush⁵, Karli Lytle⁵, Francesco Sassi², Francesca Cottino², Giorgia Migliardi^{1,2}, Eugenia R. Zanella^{1,2}, Dario Ribero^{7†}, Nadia Russolillo⁷, Alfredo Mellano², Andrea Muratore², Gianluca Paraluppi⁸, Mauro Salizzoni^{8,9}, Silvia Marsoni², Michael Kragh¹⁰, Johan Lantto¹⁰, Andrea Cassingena¹¹, Qing Kay Li⁴, Rachel Karchin^{4,6}, Robert Scharpf⁴, Andrea Sartore-Bianchi¹¹, Salvatore Siena^{11,12}, Luis A. Diaz Jr^{4,13}, Livio Trusolino^{1,2§} & Victor E. Velculescu^{4§}

Colorectal cancer is the third most common cancer worldwide, with 1.2 million patients diagnosed annually. In late-stage colorectal cancer, the most commonly used targeted therapies are the monoclonal antibodies cetuximab and panitumumab, which prevent epidermal growth factor receptor (EGFR) activation¹. Recent studies have identified alterations in KRAS^{2–4} and other genes^{5–13} as likely mechanisms of primary and secondary resistance to anti-EGFR antibody therapy. Despite these efforts, additional mechanisms of resistance to EGFR blockade are thought to be present in colorectal cancer and little is known about determinants of sensitivity to this therapy. To examine the effect of somatic genetic changes in colorectal cancer on response to anti-EGFR antibody therapy, here we perform complete exome sequence and copy number analyses of 129 patient-derived tumour grafts and targeted genomic analyses of 55 patient tumours, all of which were KRAS wild-type. We analysed the response of tumours to anti-EGFR antibody blockade in tumour graft models and in clinical settings and functionally linked therapeutic responses to mutational data. In addition to previously identified genes, we detected mutations in ERBB2, EGFR, FGFR1, PDGFRA, and MAP2K1 as potential mechanisms of primary resistance to this therapy. Novel alterations in the ectodomain of EGFR were identified in patients with acquired resistance to EGFR blockade. Amplifications and sequence changes in the tyrosine kinase receptor adaptor gene IRS2 were identified in tumours with increased sensitivity to anti-EGFR therapy. Therapeutic resistance to EGFR blockade could be overcome in tumour graft models through combinatorial therapies targeting actionable genes. These analyses provide a systematic approach to evaluating response to targeted therapies in human cancer, highlight new mechanisms of responsiveness to anti-EGFR therapies, and delineate new avenues for intervention in managing colorectal cancer.

To examine genetic alterations that affect response to anti-EGFR therapy, we selected 137 colorectal cancers (CRCs) from liver metastases that were KRAS wild-type as determined by Sanger sequencing (Supplementary Table 1). To elucidate genetic alterations in these cancers, we enriched for neoplastic cells using patient-derived tumour grafts and performed exome sequencing of tumour graft and matched normal DNA (Supplementary Tables 1 and 2). This approach identified sequence changes and copy number alterations in more than 20,000

genes, with an average coverage within the target regions of nearly 150-fold for each sample (Supplementary Tables 3 and 4).

Sequence analyses of 135 of 137 tumours identified a median of 117 somatic mutations in each cancer. Two tumours displayed an elevated number of somatic alterations (2,979 and 2,480 changes per exome), consistent with a mutator phenotype. Common CRC driver genes were identified at expected frequencies in the tumours analysed (Supplementary Tables 3–5). Eight tumours were identified as having KRAS alterations that were not initially detected by Sanger sequencing and were excluded from further analysis, resulting in 129 KRAS wild-type tumours.

To evaluate whether identified alterations were associated with resistance to EGFR inhibitors, we determined tumour graft response to cetuximab therapy for 116 of the 129 KRAS wild-type CRCs (Figs 1 and 2). The volume of each tumour graft was evaluated at 3 and 6 weeks, and tumours were categorized as showing disease progression, regression, or stabilization. Among tumour grafts with disease progression (increase in tumour volumes over 35%) or suboptimal stabilization (increase in tumour volumes between 20 and 35%), we detected alterations in all genes thought to be involved in EGFR therapeutic resistance: NRAS codon 12 or 61 mutations (seven cases), BRAF V600E mutation (three cases), MET amplification (three cases), and ERBB2 amplification (four of five cases). Additionally, three out of four tumours with alterations in exon 20 of PIK3CA and four out of five tumours with protein truncating or homozygous deletions of PTEN were resistant to anti-EGFR blockade.

We evaluated potential mechanisms of resistance that have not been previously described in CRC. We focused on cell-surface receptors or members of the EGFR signalling pathway to identify candidate genes that were altered in therapy-resistant tumours (Fig. 2, Extended Data Fig. 1 and Supplementary Tables 3 and 4). We observed point mutations affecting the ERBB2 kinase domain, including in two tumours with the same change at V777L and another tumour harbouring an L866M mutation, as well as a sequence change in the ectodomain at S310Y, all of which correlated with cetuximab resistance. Although amplification of ERBB2 has been reported in CRCs^{9,10,14}, sequence alterations in this gene have not been linked to therapeutic resistance to anti-EGFR blockade. These data suggest that somatic mutations in ERBB2 may provide an alternative mechanism for ERBB2 pathway activation that is complementary to ERBB2 amplification in CRC. Similarly, we found sequence alteration in the kinase domain of

¹Department of Oncology, University of Turin Medical School, 10060 Candiolo, Turin, Italy. ²Translational Cancer Medicine, Surgical Oncology, and Clinical Trials Coordination, Candiolo Cancer Institute—Fondazione del Piemonte per l’Oncologia IRCCS, 10060 Candiolo, Turin, Italy. ³National Institute of Biostructures and Biosystems (INBB), 00136 Rome, Italy. ⁴Sidney Kimmel Comprehensive Cancer Center, Johns Hopkins University School of Medicine, Baltimore, Maryland 21287, USA. ⁵Personal Genome Diagnostics, Baltimore, Maryland 21224, USA. ⁶Department of Biomedical Engineering, Institute for Computational Medicine, Johns Hopkins University, Baltimore, Maryland 21204, USA. ⁷Department of Surgery, Mauriziano Umberto I Hospital, 10128 Turin, Italy. ⁸Liver Transplantation Center, San Giovanni Battista Hospital, 10126 Turin, Italy. ⁹Department of Surgical Sciences, University of Turin Medical School, 10126 Turin, Italy. ¹⁰Sympogen A/S, 2750 Ballerup, Denmark. ¹¹Niguarda Cancer Center, Ospedale Niguarda Ca’ Granda, 20162 Milan, Italy. ¹²University of Milan Medical School, 20162 Milan, Italy. ¹³Swim Across America Laboratory, The Ludwig Center for Cancer Genetics and Therapeutics at Johns Hopkins, Baltimore, Maryland 21287, USA. [†]Present address: European Institute of Oncology (IEO), 20141 Milan, Italy.

*These authors contributed equally to this work.

§These authors jointly supervised this work.

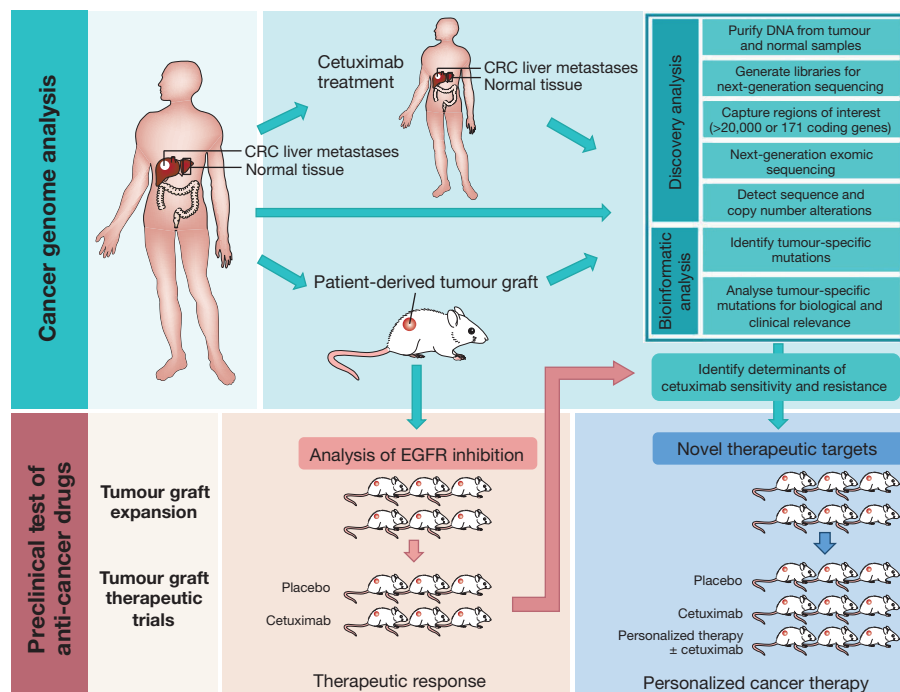


Figure 1 | Schematic diagram of integrated genomic and therapeutic analyses. To examine the effect of genomic alterations on sensitivity to anti-EGFR blockade, we performed whole-exome and copy-number analyses of 129 early-passage tumour grafts and targeted analyses of 55 tumours from patients, all of which were KRAS wild-type (top). Twenty-two of the tumour grafts were from patients who had been previously treated with anti-EGFR therapy.

One hundred and sixteen of these tumour grafts were evaluated for response to cetuximab in preclinical therapeutic trials (bottom left). Integration of genomic and therapeutic information was used to identify candidate resistance and response genes, and to design preclinical trials using novel compounds to overcome resistance to EGFR blockade (bottom right).

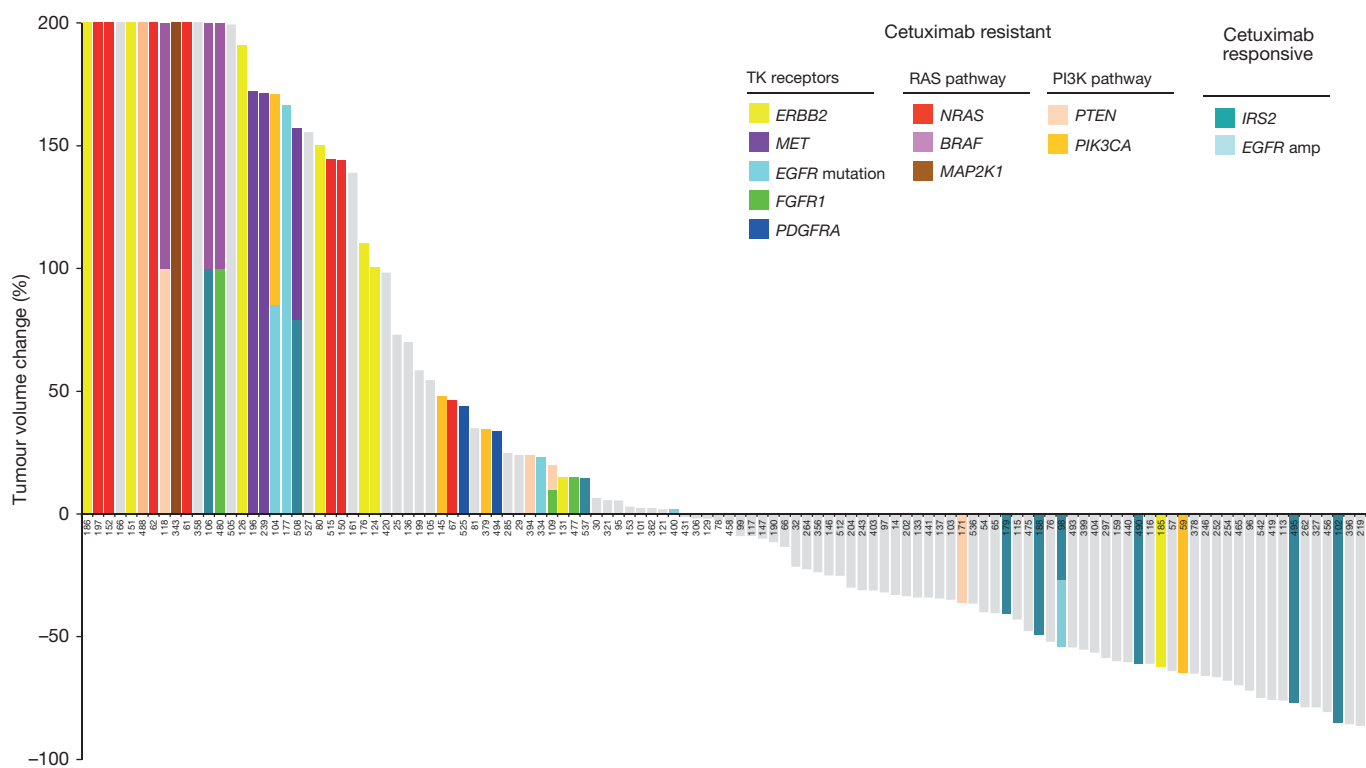


Figure 2 | Effect of cetuximab treatment on growth of colorectal tumours with different somatic alterations. Waterfall plot of tumour volume changes after cetuximab treatment, compared with baseline, in 116 KRAS wild-type tumour grafts. Alterations related to therapeutic resistance or sensitivity are shown in the indicated colours (complete lists of alterations are in Supplementary Tables 3, 4 and 6). For the following genes, a subset of

alterations is indicated: MET amplification; FGFR1 amplification; PDGFRA kinase domain mutations; BRAF V600 hotspot mutations; PTEN homozygous deletion or truncating mutations; PIK3CA exon 20 mutations; EGFR ecto- and kinase domain mutations and amplifications. The maximum threshold for tumour growth was set at 200%.

EGFR (V843I) in one case that showed tumour growth in the presence of cetuximab. Although EGFR kinase alterations are rare in CRC^{15,16}, the observed case suggests that in principle such changes may provide a mechanism of resistance to anti-EGFR therapy.

We identified alterations in additional protein kinase receptors in tumours resistant to cetuximab treatment: amplification of the fibroblast growth factor receptor *FGFR1* and sequence alterations in the platelet-derived growth factor receptor *PDGFRA*. Each of these was altered in four of the 129 CRC samples analysed (8 samples in total, 6%). *FGFR1* is a known driver in human cancers¹⁷ and has been reported to be amplified in different tumour types. *PDGFRA* is a tyrosine kinase receptor that is known to be mutated in gastrointestinal stromal tumours¹⁸. The detected sequence alterations in *PDGFRA*, including a mutation that affected the same residue in two different patients (R981H), were all located in or near the catalytic domain of the protein. Similar to *ERBB2* and *MET*, the receptors encoded by these genes transmit signals through the RAS/MEK cascade and when mutated can lead to constitutive activation of oncogenic pathways^{17,19}.

We further examined candidate alterations within the RAS pathway and observed a K57R change in the mitogen-activated protein kinase gene *MAP2K1* in a cetuximab-resistant case. Alterations of *MAP2K1* at the same or nearby residues have been previously described in various cancers, are adjacent to the catalytic domain, and have been shown to confer IL-3-independent cell growth *in vitro*, suggesting that this mutation may be functionally active²⁰. Overall, the enrichment of mutations in these pathways in the resistant tumour grafts was statistically significant ($P < 0.001$, Welch's two-sample *t*-test) and suggests that alterations in any of these members may be sufficient to render cells insensitive to EGFR inhibition.

To extend the observations, we analysed 65 cetuximab-naïve samples from patients who were subsequently treated with anti-EGFR therapy as part of clinical trials or standard of care. We detected coding alterations in genes known to be involved in EGFR therapeutic resistance, including *KRAS*, *NRAS*, *BRAF*, *PIK3CA*, and *PTEN* sequence mutations, and amplification of *MET* and *ERBB2* (a total of 25 cases with mutation in at least one resistance gene). In the remaining 40 cases, we confirmed observations of alterations in several genes with novel resistance mechanisms, including sequence changes in *ERBB2* and *PDGFRA* (Supplementary Tables 1–3).

Although some tumours respond to cetuximab, virtually all patients with CRC develop disease recurrence. In our analyses, 22 tumours were from patients who received cetuximab within 6 months before resection (Supplementary Table 1). We examined whether alterations in these cases may have arisen as acquired (secondary) resistance to therapy. Two of these 22 tumours had somatic sequence changes in *EGFR* (G465R or G465E) affecting domain III of the extracellular portion of the receptor. Structural analyses suggested that these mutations were likely to affect cetuximab binding as they were located at the interface of EGFR–cetuximab interaction (Fig. 3a and Extended Data Fig. 2). Interestingly, G465 is structurally adjacent to residue S492 that has been shown, when altered, to interfere with cetuximab binding¹¹ (Fig. 3a). We sequenced pre- and post-therapy specimens for the two patients (CRC104 and CRC177) whose tumours harboured the ectodomain mutations. In both cases, we confirmed the *EGFR* mutations in the post-cetuximab metastases while the original pre-treatment specimens did not have detectable alterations (Fig. 3b, c).

Among patients with CRC with *KRAS* wild-type tumours, only 12–17% have durable responses to anti-EGFR monotherapy^{4,6}. We wondered whether such responses may be due to alterations in genes that confer therapeutic sensitivity. *EGFR* was found to be amplified in two tumours that showed either regression (CRC98, 26-fold amplified) or disease stabilization (CRC400, 3-fold amplified) (Fig. 2), consistent with previous observations^{21,22}. Given the importance of EGFR signalling in CRC, we analysed other pathway members that were preferentially mutated in responsive tumours and identified *IRS2*, a cytoplasmic adaptor that mediates signalling between receptor

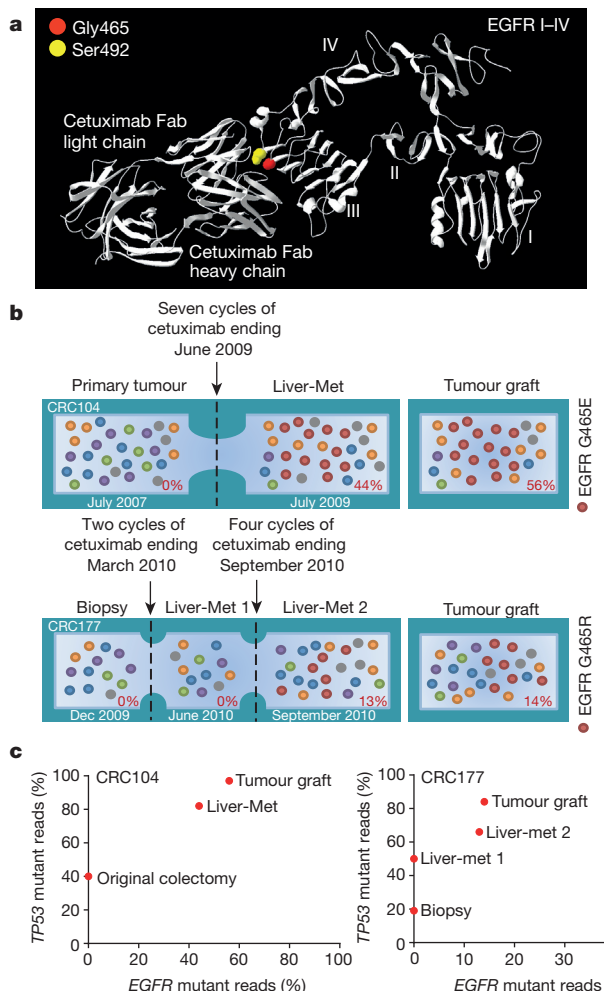


Figure 3 | Genetic alterations involved in secondary resistance to anti-EGFR therapy. **a**, The locations of mutations in *EGFR* ectodomain are shown including G465 (red) and the S492 residue known to confer cetuximab resistance¹¹ (yellow). **b**, Evolution of *EGFR* mutations in two CRCs with acquired resistance to cetuximab. Cetuximab-naïve samples were sequenced to investigate the presence of *EGFR* G465 mutations (red) before treatment. For each sample, the fraction of mutant tags is indicated. Met, metastases. **c**, As a control for tumour cellularity, for each lesion the fraction of *TP53* mutant reads (vertical axis) was plotted against the fraction of reads with *EGFR* ectodomain mutations (horizontal axis).

tyrosine kinases and downstream targets (Fig. 2 and Supplementary Table 6) ($P < 0.05$, Welch's two-sample *t*-test). *IRS2* had amplifications or sequence alterations in seven tumours (10%) that showed increased sensitivity or stable disease when treated with cetuximab. Expression analyses of 100 CRC tumour grafts with wild-type *KRAS*, *NRAS*, *BRAF*, and *PIK3CA* identified increased *IRS2* levels as a significant predictor of cetuximab sensitivity (Extended Data Fig. 3). A few tumours that were not responsive to cetuximab harboured *IRS2* alterations together with known resistance changes, including those in *MET* or *BRAF*. These observations suggest that *IRS2* mutations may predict anti-EGFR sensitivity in cases without other mechanisms of resistance to EGFR therapy. We and others have previously identified alterations in *IRS2* in CRCs and other tumour types, but no reports so far have linked the effects of these alterations to therapeutic sensitivity^{14,23}.

To evaluate the role of these novel alterations, we performed functional assays in NCI-H508, a cetuximab-sensitive CRC cell line that does not harbour known resistance-conferring mutations^{24,25} and displays a threefold gene copy number gain of the *IRS2* gene (Supplementary Tables 3 and 4). We found that ectopic introduction of either *EGFR* G465E or *MAP2K1* K57N into NCI-H508 cells induced resistance to

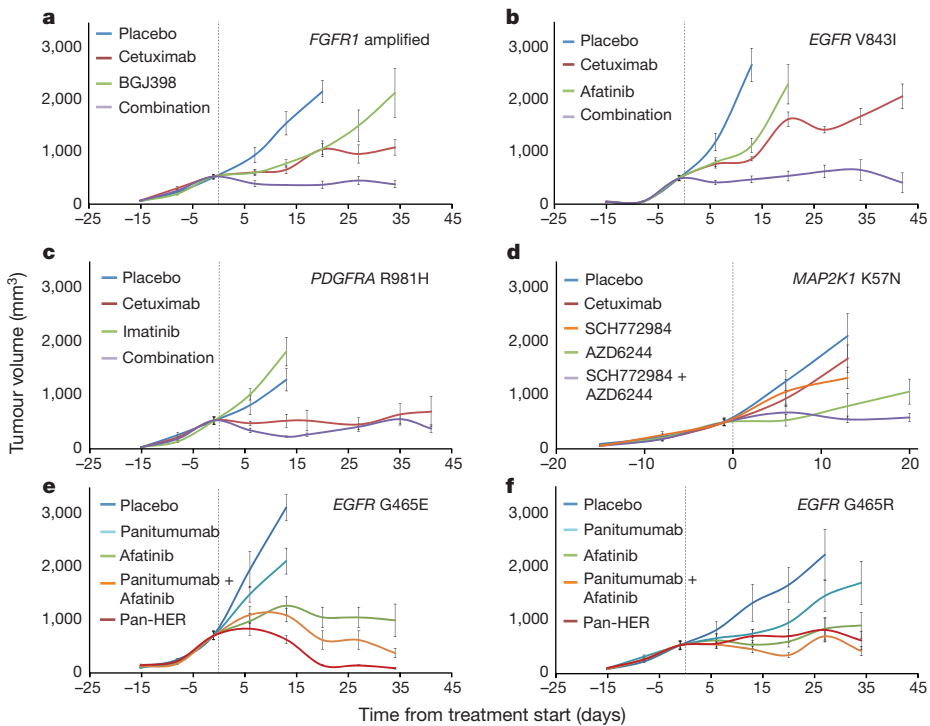


Figure 4 | Therapeutic intervention in preclinical trials to overcome resistance to anti-EGFR antibody blockade. **a–f,** Tumour growth curves in tumour graft cohorts from individual patients with *FGFR1* amplification (CRC477) (**a**), *EGFR* kinase mutation (CRC334) (**b**), *PDGFRA R981H* mutation (CRC525) (**c**), *MAP2K1 K57N* mutation (CRC343) (**d**), and *EGFR* ectodomain mutations (**e**, CRC104; **f**, CRC177) treated with placebo or targeted treatments. Mean tumour volumes \pm s.e.m. are shown ($n = 5$ mice per

EGFR inhibition and increased activation of downstream signals, which were not affected by EGFR blockade (Extended Data Fig. 4a, b). Conversely, knockdown of IRS2 by short hairpin RNA (shRNA) resulted in reduced sensitivity to cetuximab and less pronounced activation of ERK and AKT following ligand stimulation (Extended Data Fig. 4c). This is consistent with the role of IRS2 as a scaffold/adaptor protein that amplifies signals downstream from tyrosine kinase receptors.

Given the poor outcome of patients diagnosed with late-stage CRC, we investigated whether mutant genes observed in individual cases may be clinically actionable using existing or investigational therapies. We identified somatic alterations with potentially actionable consequences in 100 of the 129 patients (77%) (Supplementary Table 8). To test whether any of the identified alterations could be successfully targeted in tumours with cetuximab resistance, we used the tumour grafts to perform proof-of-principle trials for targeted therapies and evaluated the signalling consequences of these therapies *in vivo* (Fig. 4 and Extended Data Figs 5–10). We chose a cetuximab-resistant tumour with *FGFR1* amplification (CRC477) and examined whether inhibition of both *FGFR1* and *EGFR* would be more effective than inhibition of *EGFR* alone. We confirmed resistance to cetuximab alone and, as may be expected using a single inhibitor, the tumour graft was also resistant to monotherapy with the selective *FGFR* kinase inhibitor BGJ398, which is currently in clinical trials (Fig. 4a). However, combination of BGJ398 with cetuximab led to a substantial and durable suppression of tumour growth in all treated mice. This model confirmed that combinatorial therapies may be effective in overcoming *EGFR* therapeutic resistance in tumours with alterations in other cell-surface receptors.

An analogous approach was used to evaluate the *EGFR* small-molecule inhibitor afatinib in tumour CRC334 containing sequence change V843I in the protein kinase domain of *EGFR*. Similar to our observations for *FGFR1* targeting, treating tumour grafts with afatinib or cetuximab alone was not effective but the combination resulted in

group for CRC525 and CRC177; $n = 6$ mice per group for all other models). **a, b,** Combination versus cetuximab, $P < 0.01$; **c,** combination versus cetuximab, not significant; **d,** SCH772984 + AZD6244 versus either monotherapy, $P < 0.01$; **e, f,** afatinib, Pan-HER or panitumumab + afatinib versus panitumumab, $P < 0.01$. Statistical analysis was performed by two-way analysis of variance (ANOVA).

marked and long-lasting inhibition of tumour growth (Fig. 4b). We also found that combinations of MEK and ERK inhibitors in tumour graft CRC343 (*MAP2K1 K57N*), and the PDGFR inhibitor imatinib and cetuximab in tumour graft CRC525 (*PDGFRA R981H*), exerted strong anti-tumour activities (Fig. 4c, d), although the effect was short-lived in the *PDGFRA* mutant tumour. Targeting of *ERBB2* mutations in cetuximab-resistant CRC tumour grafts has been recently demonstrated using dual HER2-targeted therapy in a separate study²⁶. Consistent with the observed higher efficacy of combination therapies, we found that the impact of therapies on downstream signals was stronger when tumours were targeted by drug combinations compared with single-agent treatments (Extended Data Figs 5–10).

Next, we evaluated alternative therapeutic approaches in tumours with secondary cetuximab-resistant alterations in the *EGFR* ectodomain. Although previous reports have shown that cetuximab-resistant tumours with S492R alterations in *EGFR* are sensitive to panitumumab¹¹, tumour grafts with the *EGFR G465E* mutation were poorly sensitive to panitumumab (Fig. 4e). Structural analyses indicate that the S492 residue is in the cetuximab binding site within *EGFR* domain III, while G465 is located in the centre of the region in which the epitopes of both antibodies overlap²⁷ (Extended Data Fig. 2). This lack of sensitivity was not due to absence of *EGFR* dependence as kinase inhibition of *EGFR* using afatinib resulted in reduction of tumour growth (Fig. 4e). To explore whether *EGFR* inhibition by antibodies targeting epitopes far from G465 might overcome resistance, we used Pan-HER (Symphogen), a monoclonal antibody mixture that binds *EGFR* epitopes different from those recognized by cetuximab and panitumumab²⁸ (Extended Data Fig. 2). Pan-HER displayed strong anti-tumour activity in both CRC104 with the *EGFR G465E* mutation (Fig. 4e) and CRC177 with the *EGFR G465R* mutation (Fig. 4f).

Our genomic analyses have detected essentially all previously known mechanisms of resistance to cetuximab in CRC. The results

identify novel candidate mechanisms of primary and secondary resistance through alterations affecting *EGFR*, its downstream signalling pathway, and other cell-surface receptors (Extended Data Fig. 1). These alterations, together with *KRAS*, constitute over three-quarters of cetuximab-resistant tumours and suggest that the vast majority of mechanisms of primary resistance have now been determined and can be identified before the initiation of anti-*EGFR* treatment.

Some of the mechanisms of resistance to *EGFR* therapy provide new avenues for intervention, including amplification of *FGFR1* and mutations of *PDGFR1*, *ERBB2*, and *MAP2K1*. As we have shown, combinations of therapies targeting both the protein products encoded by resistance genes as well as *EGFR* or other signalling partners are likely to be crucial for inhibiting the multiple genetic components within a tumour. Although combinatorial treatments in tumour grafts often led to arrest of tumour growth rather than regression, disease stabilization is prognostically relevant and is the most common consequence of *EGFR*-targeted therapies in responsive patients with CRC⁴. The high fraction of tumours with actionable alterations suggests that additional combinatorial therapies may be clinically useful for patients with CRC.

An unexpected finding was the identification of *IRS2* alterations as a novel mechanism of sensitivity to anti-*EGFR* therapy. Our genetic and functional data suggest that *IRS2* alterations may identify tumours that are dependent on receptor signalling and therefore sensitive to its therapeutic inhibition. Consistent with this prediction are reports that *IRS2* amplification is a significant indicator of response to the *IGF1R* inhibitor figtumumab in colorectal and lung cancer cell lines²⁹. Given the interaction of *IRS2* with multiple cell-surface receptors, we would predict that combinatorial inhibition of these receptors in tumours with *IRS2* alterations may provide additional avenues of intervention in such patients.

This study highlights information that may be obtained through the integration of large-scale genomic and targeted therapeutic analyses in CRC. It provides an unprecedented view into mechanisms of sensitivity as well as primary and secondary resistance to *EGFR* blockade. This information gives a framework for analysis of responses to targeted therapies in CRC and suggests interventional clinical trials using combinatorial therapies based on potentially actionable alterations.

Online Content Methods, along with any additional Extended Data display items and Source Data, are available in the online version of the paper; references unique to these sections appear only in the online paper.

Received 17 November 2014; accepted 22 July 2015.

Published online 30 September 2015.

- Van Cutsem, E., Cervantes, A., Nordlinger, B. & Arnold, D. on behalf of the ESMO Guidelines Working Group. Metastatic colorectal cancer: ESMO Clinical Practice Guidelines for diagnosis, treatment and follow-up. *Ann. Oncol.* **25** (Suppl. 3), iii1–iii9 (2014).
- Diaz, L. A. Jr et al. The molecular evolution of acquired resistance to targeted *EGFR* blockade in colorectal cancers. *Nature* **486**, 537–540 (2012).
- Misale, S. et al. Emergence of *KRAS* mutations and acquired resistance to anti-*EGFR* therapy in colorectal cancer. *Nature* **486**, 532–536 (2012).
- Amado, R. G. et al. Wild-type *KRAS* is required for panitumumab efficacy in patients with metastatic colorectal cancer. *J. Clin. Oncol.* **26**, 1626–1634 (2008).
- De Roock, W. et al. Effects of *KRAS*, *BRAF*, *NRAS*, and *PIK3CA* mutations on the efficacy of cetuximab plus chemotherapy in chemotherapy-refractory metastatic colorectal cancer: a retrospective consortium analysis. *Lancet Oncol.* **11**, 753–762 (2010).
- Tol, J. et al. Markers for *EGFR* pathway activation as predictor of outcome in metastatic colorectal cancer patients treated with or without cetuximab. *Eur. J. Cancer* **46**, 1997–2009 (2010).
- Sartore-Bianchi, A. et al. *PIK3CA* mutations in colorectal cancer are associated with clinical resistance to *EGFR*-targeted monoclonal antibodies. *Cancer Res.* **69**, 1851–1857 (2009).
- Bardelli, A. et al. Amplification of the *MET* receptor drives resistance to anti-*EGFR* therapies in colorectal cancer. *Cancer Discov.* **3**, 658–673 (2013).
- Bertotti, A. et al. A molecularly annotated platform of patient-derived xenografts ("xenobodies") identifies *HER2* as an effective therapeutic target in cetuximab-resistant colorectal cancer. *Cancer Discov.* **1**, 508–523 (2011).
- Yonesaka, K. et al. Activation of *ERBB2* signalling causes resistance to the *EGFR*-directed therapeutic antibody cetuximab. *Sci. Transl. Med.* **3**, 99ra86 (2011).

- Montagut, C. et al. Identification of a mutation in the extracellular domain of the epidermal growth factor receptor conferring cetuximab resistance in colorectal cancer. *Nature Med.* **18**, 221–223 (2012).
- Bettegowda, C. et al. Detection of circulating tumor DNA in early- and late-stage human malignancies. *Sci. Transl. Med.* **6**, 224ra224 (2014).
- Diaz, L. A. Jr, Sausen, M., Fisher, G. A. & Velculescu, V. E. Insights into therapeutic resistance from whole-genome analyses of circulating tumor DNA. *Oncotarget* **4**, 1856–1857 (2013).
- Leary, R. J. et al. Integrated analysis of homozygous deletions, focal amplifications, and sequence alterations in breast and colorectal cancers. *Proc. Natl. Acad. Sci. USA* **105**, 16224–16229 (2008).
- Barber, T. D., Vogelstein, B., Kinzler, K. W. & Velculescu, V. E. Somatic mutations of *EGFR* in colorectal cancers and glioblastomas. *N. Engl. J. Med.* **351**, 2883 (2004).
- Moroni, M. et al. Somatic mutation of *EGFR* catalytic domain and treatment with gefitinib in colorectal cancer. *Ann. Oncol.* **16**, 1848–1849 (2005).
- Wesche, J., Haglund, K. & Haugsten, E. M. Fibroblast growth factors and their receptors in cancer. *Biochem. J.* **437**, 199–213 (2011).
- Heinrich, M. C. et al. PDGFRA activating mutations in gastrointestinal stromal tumors. *Science* **299**, 708–710 (2003).
- Dibb, N. J., Dilworth, S. M. & Mol, C. D. Switching on kinases: oncogenic activation of *BRAF* and the PDGFR family. *Nature Rev. Cancer* **4**, 718–727 (2004).
- Marks, J. L. et al. Novel *MEK1* mutation identified by mutational analysis of epidermal growth factor receptor signaling pathway genes in lung adenocarcinoma. *Cancer Res.* **68**, 5524–5528 (2008).
- Algars, A., Lintunen, M., Carpen, O., Ristamaki, R. & Sundstrom, J. EGFR gene copy number assessment from areas with highest EGFR expression predicts response to anti-EGFR therapy in colorectal cancer. *Br. J. Cancer* **105**, 255–262 (2011).
- Moroni, M. et al. Gene copy number for epidermal growth factor receptor (EGFR) and clinical response to anti-EGFR treatment in colorectal cancer: a cohort study. *Lancet Oncol.* **6**, 279–286 (2005).
- Parsons, D. W. et al. Colorectal cancer: mutations in a signalling pathway. *Nature* **436**, 792 (2005).
- Misale, S. et al. Blockade of EGFR and MEK intercepts heterogeneous mechanisms of acquired resistance to anti-EGFR therapies in colorectal cancer. *Sci. Transl. Med.* **6**, 224ra226 (2014).
- Zanella, E. R. et al. IGF2 is an actionable target that identifies a distinct subpopulation of colorectal cancer patients with marginal response to anti-EGFR therapies. *Sci. Transl. Med.* **7**, 272ra212 (2015).
- Kavuri, S. M. et al. HER2 activating mutations are targets for colorectal cancer treatment. *Cancer Discov.* **5**, 832–841 (2015).
- Voigt, M. et al. Functional dissection of the epidermal growth factor receptor epitopes targeted by panitumumab and cetuximab. *Neoplasia* **14**, 1023–1031 (2012).
- Koefoed, K. et al. Rational identification of an optimal antibody mixture for targeting the epidermal growth factor receptor. *MAbs* **3**, 584–595 (2011).
- Pavlicek, A. et al. Molecular predictors of sensitivity to the insulin-like growth factor 1 receptor inhibitor Figitumumab (CP-751,871). *Mol. Cancer Ther.* **12**, 2929–2939 (2013).

Supplementary Information is available in the online version of the paper.

Acknowledgements We thank S. Angioli, D. Riley, L. Kann, M. Shukla, and C. L. McCord for their assistance with next-generation sequencing analyses, and F. Galimi and S. M. Leto for their help with Sanger sequencing analyses and functional studies. This work was supported by the John G. Ballenger Trust, FasterCures Research Acceleration Award, the European Community's Seventh Framework Programme, the AIRC Italian Association for Cancer Research (Special Program Molecular Clinical Oncology 5×1000, project 9970, and Investigator Grants projects 14205 and 15571), American Association for Cancer Research (AACR) – Fight Colorectal Cancer Career Development Award in memory of Lisa Dubow (project 12-20-16-BERT), the Commonwealth Foundation, Swim Across America, US National Institutes of Health grant CA121113, Fondazione Piemontese per la Ricerca sul Cancro-ONLUS (5×1000 Italian Ministry of Health 2011), Oncologia Ca' Granda ONLUS, and the SU2C-DCS International Translational Cancer Research Dream Team Grant (SU2C-AACR-DT1415). We acknowledge Merck for a gift of cetuximab. Stand Up To Cancer is a program of the Entertainment Industry Foundation administered by the American Association for Cancer Research. A.B. and L.T. are members of the EurOPDX Consortium.

Author Contributions A.B. and E.P. conceived the project, designed and performed experiments, interpreted results and co-wrote the manuscript. S.J., V.A., V.A., B.L., M.S., J.P., C.A.H., M.N., K.L., F.S., F.C., G.M., E.R.Z., D.R., N.R., A.M., A.M., G.P., M.S., S.M., and A.C. performed experiments, analysed data, prepared tables, or participated in discussion of the results. M.K. and J.L. contributed reagents. Q.K.L. undertook all pathological evaluations. C.T., N.N., R.K., and R.S. performed statistical analyses. A.S.-B., S.S., and L.A.D. provided clinically annotated samples and supervised experimental designs. L.T. and V.E.V. conceived the project, supervised experimental designs, interpreted results, and co-wrote the manuscript.

Author Information Sequence data have been deposited at the European Genome-phenome Archive, which is hosted at the European Bioinformatics Institute, under study accession EGAS00001001305. Reprints and permissions information is available at www.nature.com/reprints. The authors declare competing financial interests: details are available in the online version of the paper. Readers are welcome to comment on the online version of the paper. Correspondence and requests for materials should be addressed to V.E.V. (velculescu@jhmi.edu), L.T. (livio.trusolino@irc.citt.it) or A.B. (andrea.bertotti@irc.citt.it).

METHODS

Specimens obtained for sequencing analysis. The study population consisted of matched tumour and normal samples from 137 patients with CRC who underwent surgical resection of liver metastases at the Candiolo Cancer Institute, the Mauriziano Umberto I Hospital and the San Giovanni Battista Hospital (all Turin) from 2008 to 2012. Informed consent for research use was obtained from all patients at the enrolling institution before tissue banking, and study approval was obtained from the ethics committees of the three centres. Tumours with KRAS alterations at codons 12, 13, and 61 that were detected using Sanger sequencing were not included in the study. From the resected tumour samples, tumour graft models were established as described below. Following exome sequence analyses, eight tumour grafts were detected to have KRAS mutations (patients CRC18, CRC58, CRC68, CRC237, CRC312, CRC328, CRC344, CRC382) and were excluded from further analyses. To assess genomic similarity between tumour grafts and the tumours from which they were derived, 18 pre-implantation liver metastases were analysed through targeted next-generation sequencing and compared with the corresponding tumour grafts. Pathological analyses showed that tumour cellularity of the metastatic samples ranged from 15% to 90% (average 59%), supporting the need for enrichment of tumour cells through growth of tumour grafts. Targeted next-generation sequencing revealed that all the clonal alterations identified in these tumour grafts were present in the tumours from which they were derived (Supplementary Table 3), similar to previous comparisons of tumour grafts and primary tumours in CRC³⁰. To extend observations of alterations in resistance mechanisms that we had identified in tumour grafts, an additional 65 patient-derived cetuximab-naïve clinical samples from patients who were subsequently treated with EGFR blockade through standard of care or various clinical trials, including NCT00113763, NCT00891930, NCT00113776, and NCT01126450 (ref. 31), were analysed through targeted genomic analyses (Supplementary Table 9). Available clinical information for all samples is shown in Supplementary Table 2.

Tumour graft models and *in vivo* treatments. Tissue from hepatic metastasectomy in affected individuals was fragmented and either frozen or prepared for implantation as described previously^{9,32}. Non-obese diabetic/severe combined immunodeficient (NOD/SCID) female mice (4–6 weeks old) were used for tumour implantation. Nucleic acids were isolated from early-passaged tumour grafts. The remaining tumour graft material was further passaged and expanded into treatment groups. The size of the animal groups ($n = 5$ or 6) and schedule of measurements (one measurement at baseline and three to five sequential weekly measurements on treatment) were calculated to detect a difference of tumour volumes between mice treated with monotherapy and mice treated with combination therapies. Therefore, three comparisons were considered as primary objective for each experiment. To preserve a family-wise error of 5% (one side), a Bonferroni correction was applied and a type 1 error of 0.017 for each of the three comparisons was considered. This resulted in a power of 80% to detect a standardized comparison of 0.70. Animals with established tumours defined as an average volume of 400 mm³ were randomized and treated with vehicle or drug regimens, either as a single-agent or in combination as indicated: cetuximab (Merck), 20 mg/kg twice a week intraperitoneally; BGJ398 (Sequoia Research Products), 30 mg/kg once-daily by oral gavage; imatinib (Sequoia Research Products), 100 mg/kg once-daily by oral gavage; panitumumab (Amgen), 20 mg/kg twice a week intraperitoneally; afatinib (Sequoia Research Products), 20 mg/kg once-daily by oral gavage; AZD6244 (Sequoia Research Products), 25 mg/kg once-daily by oral gavage; SCH772984 (ChemicTek), 75 mg/kg/once daily intraperitoneally; Pan-HER (Symphogen), 60 mg/kg twice a week intraperitoneally. To evaluate sensitivity to cetuximab monotherapy, each tumour graft was evaluated at 3 and 6 weeks in 12 or 24 mice (depending on individual models) that were randomized to treatment and control arms at a 1:1 ratio. For assessment of tumour response to therapy, we used volume measurements normalized to the tumour graft volume at the time of initiation of cetuximab treatment. Tumour grafts were classified as follows: (1) tumour regression with a decrease of at least 35% in tumour volume (39 cases, 34%); (2) disease progression with at least a 35% increase in tumour volume (36 cases, 31%); and (3) disease stabilization with a tumour graft volume at levels < 35% growth and < 35% regression (41 cases, 35%). Tumours displaying regression or stabilization continued treatment for additional 3 weeks. Tumour size was evaluated once a week by calliper measurements and the approximate volume of the mass was calculated. Statistical significance for tumour volume changes was calculated using mixed-design ANOVA (repeated measures) when all mice were available for measurements in each treatment group at each time point, and two-way ANOVA when one or more mice died accidentally over the course of the experiments. Results were considered interpretable when at least half of mice per treatment group ($n = 3$) survived until the pre-specified endpoints (minimum, 3 weeks of treatment). All mice alive at the endpoint were included in the analysis (CRC477: six mice treated with placebo or cetuximab, four mice

treated with BGJ398, three mice treated with cetuximab + BGJ398; CRC334: five mice treated with cetuximab + afatinib, six mice per treatment group in all other arms; CRC525: five mice per treatment group in all arms; CRC343: five mice treated with AZD6244 + SCH772984, six mice per treatment group in all other arms; CRC104: four mice treated with panitumumab + afatinib, six mice per treatment group in all other arms; CRC177: five mice per treatment group in all arms). Operators allocated mice to the different treatment groups during randomization but were blinded during measurements. *In vivo* procedures and related biobanking data were managed using the Laboratory Assistant Suite (LAS), a web-based proprietary data management system for automated data tracking³³. All experiments were conducted with approval from the Animal Care Committee of the Candiolo Cancer Institute, in accordance with Italian legislation on animal experimentation.

Sample preparation and next-generation sequencing. DNA was extracted from patients' tumours, early-passage tumour grafts developed from liver metastases, normal samples (adjacent non-cancerous liver or peripheral blood), and from normal tissue of the same mouse strain as those used to grow the xenografts using the Qiagen DNA FFPE tissue kit or Qiagen DNA blood mini kit. Additional analyses were performed for CRC334 after afatinib anti-EGFR therapy and tumour graft regrowth (indicated in footnote of Supplementary Table 4). Genomic DNA from tumour and normal samples were fragmented and used for Illumina TruSeq library construction (Illumina) according to the manufacturer's instructions or as previously described³⁴. Exonic or targeted regions were captured in solution using the Agilent SureSelect version 4 kit or a custom targeted panel according to the manufacturer's instructions (Agilent) (Supplementary Table 9). The captured library was then purified with a Qiagen MinElute column purification kit and eluted in 17 µl of 70 °C EB to obtain 15 µl of captured DNA library. The captured DNA library was amplified in the following way: eight 30 µl PCR reactions each containing 19 µl of H₂O, 6 µl of 5 × Phusion HF buffer, 0.6 µl of 10 mM dNTP, 1.5 µl of DMSO, 0.30 µl of Illumina PE primer 1, 0.30 µl of Illumina PE primer 2, 0.30 µl of Hotstart Phusion polymerase, and 2 µl of captured exome library were set up. The PCR program used was as follows: 98 °C for 30 s; 14 cycles (exome) or 16 cycles (targeted) of 98 °C for 10 s, 65 °C for 30 s, 72 °C for 30 s; and 72 °C for 5 min. To purify PCR products, a NucleoSpin Extract II purification kit (Macherey-Nagel) was used following the manufacturer's instructions. Paired-end sequencing, resulting in 100 bases from each end of the fragments for exome libraries and 100 or 150 bases from each end of the fragment for targeted libraries, was performed using Illumina HiSeq 2000/2500 and Illumina MiSeq instrumentation (Illumina).

Primary processing of next-generation sequencing data and identification of putative somatic mutations. Somatic mutations were identified using VariantDx³⁴ custom software for identifying mutations in matched tumour and normal samples. Before mutation calling, primary processing of sequence data both for tumour and for normal samples was performed using Illumina CASAVA software (version 1.8), including masking of adaptor sequences. Sequence reads were aligned against the human reference genome (version hg18) using ELAND with additional realignment of select regions using the Needleman-Wunsch method³⁵. Candidate somatic mutations, consisting of point mutations, insertions, and deletions, were then identified using VariantDx across the either the whole exome or regions of interest. VariantDx examines sequence alignments of tumour samples against a matched normal while applying filters to exclude alignment and sequencing artefacts. In brief, an alignment filter was applied to exclude quality failed reads, unpaired reads, and poorly mapped reads in the tumour. A base quality filter was applied to limit inclusion of bases with reported Phred quality score > 30 for the tumour and > 20 for the normal. A mutation in the tumour was identified as a candidate somatic mutation only when (1) distinct paired reads contained the mutation in the tumour, (2) the number of distinct paired reads containing a particular mutation in the tumour was at least 2% of the total distinct read pairs for targeted analyses and 10% of read pairs for exome, (3) the mismatched base was not present in > 1% of the reads in the matched normal sample as well as not present in a custom database of common germline variants derived from dbSNP, and (4) the position was covered in both the tumour and normal. Mutations arising from misplaced genome alignments, including paralogous sequences, were identified and excluded by searching the reference genome. Potential alterations were compared with mouse sequences from experimentally obtained mouse whole-exome and targeted sequence data as well as the reference mouse genome (mm9) to remove mouse-specific variants. Candidate somatic mutations were further filtered on the basis of gene annotation to identify those occurring in protein coding regions. Functional consequences were predicted using snpEff and a custom database of CCDS, RefSeq and Ensembl annotations using the latest transcript versions available on hg18 from UCSC (<https://genome.ucsc.edu/>). Predictions were ordered to prefer transcripts with canonical start and stop codons and CCDS or Refseq transcripts over Ensembl when available.

Finally, mutations were filtered to exclude intronic and silent changes, while retaining mutations resulting in missense mutations, nonsense mutations, frame-shifts, or splice-site alterations. A manual visual inspection step was used to further remove artefactual changes. Amplification analyses were performed using the digital karyotyping approach³⁶ by comparing the number of reads mapping to a particular gene with the average number of reads mapping to each gene in the panel, along with a minor allele fraction analysis of heterozygous single nucleotide polymorphisms contained within each gene. For comparison of somatic alterations in tumour graft and pre-implantation material, we considered all alterations where the mutation was present in at least 20% of the read pairs in the tumour graft samples. To evaluate whether mutant genes observed in individual cases could be clinically actionable using existing or investigational therapies, we examined altered genes that were associated with (1) US Food and Drug Administration-approved therapies for oncological indications, (2) therapies in published prospective or retrospective clinical studies, and (3) ongoing clinical trials for patients with CRC or other tumour types.

Gene expression analyses. Data were obtained using a HumanHT-12 version 4 Illumina beadarray technology. Following data normalization, genes were collapsed to the probe displaying highest mean signal. Gene expression values were then log₂-transformed and centred to the median (Supplementary Table 10). IRS2 expression in 100 tumour grafts with wild-type forms of KRAS, NRAS, BRAF, and PIK3CA was compared with cetuximab response by one-way ANOVA and Bonferroni's multiple comparisons test.

Statistical analyses for genes with somatic alterations. Using the approach previously described³⁷, we analysed 24,334 somatic mutations (non-synonymous and synonymous single-base substitutions plus indels) identified in the protein coding sequence of 127 tumour graft samples, after samples with KRAS hotspot mutations (codons 12 or 13) and those with a mutator phenotype were excluded. We implemented the following statistical framework to identify significantly mutated genes by incorporating background mutation rates, gene length, and base composition.

Inspired by previous works^{38,39}, our model defines gene-specific background mutation rates, which capture exome-wide as well as gene-specific sequence-based parameters. We define eight exhaustive and disjoint sequence-based dinucleotide contexts: C in CpG, G in CpG, C in TpC, G in GpA, and all other A, G, C, T. We represent the occurrences of each context in the entire protein coding sequence by N_i , and in each gene of interest by g_i . Subsequently, we identify the dinucleotide context for all single-base substitution somatic mutations identified and derive the counts of mutations in each context over all CDS (protein coding sequence) (n_i). We derive the expected probability of observing a mutation in a base occurring in the CDS of a gene of interest as follows:

$$P_{\text{mut}} = \frac{\sum_{i=1}^I g_i f_i}{\sum_{i=1}^I g_i} \quad (1)$$

$$f_i = \frac{n_i}{N_i} \quad (2)$$

where f_i denotes the fraction of bases in dinucleotide context i in the entire CDS, where a mutation has been observed. The context parameters N_i and g_i are defined as the total number of occurrences of each context sequenced across all of the samples; therefore following the simplifying assumption of full coverage of the entire protein coding sequence, and assuming K samples total, these parameters will be K times those of a single haploid exome.

Following the definition of f_i , we derive the background probability of observing at least $m_{g,\text{obs}}$ mutations in a gene of interest, using the binomial tail probability of L_g trials with $m_{g,\text{obs}}$ successes and P_{mut} probability of success in each trial. Here, L_g represents the length of the CDS of the gene times the number of samples.

$$P_{\text{freq}}^{\text{mut}} = P(m_{g,\text{mut}} \geq m_{g,\text{obs}}) = \sum_{j=m_{g,\text{obs}}}^{L_g} \binom{L_g}{j} P_{\text{mut}}^j (1 - P_{\text{mut}})^{L_g - j} \quad (3)$$

We use an equivalent formulation to model the statistical significance of observing $q_{g,\text{obs}}$ insertions/deletions (indels) in a gene of interest. The background indel frequency (P_{indel}) is defined as the number of indels recovered in the entire CDS of the sequenced samples divided by the length of the entire CDS available in these samples.

$$P_{\text{freq}}^{\text{indel}} = P(q_{g,\text{indel}} \geq q_{g,\text{obs}}) = \sum_{j=q_{g,\text{obs}}}^{L_g} \binom{L_g}{j} P_{\text{indel}}^j (1 - P_{\text{indel}})^{L_g - j} \quad (4)$$

The two statistical tests described above (equations (3 and 4)) reflect the significance of mutation counts in a gene, but are blind to the protein-level consequence of mutations. To capture the impact of mutation on protein, we apply an extension of the tests above that examines enrichment for non-synonymous mutations in the

set of single-base substitution mutations identified in a gene of interest. We define a background, gene-specific ratio of non-synonymous to synonymous (NS/S) mutations, given the exome-wide NS/S ratio in each dinucleotide context (r_i) and the sequence composition of each gene as follows. Note that g_i has the same definition as in equation (1).

$$r_g = \frac{\sum_{i=1}^I r_i g_i}{\sum_{i=1}^I g_i} \quad (5)$$

Given the NS/S ratio for a gene of interest, the probability of an observed mutation in the gene being non-synonymous is

$$P_{g,\text{NS}} = \frac{r_g}{(r_g + 1)} \quad (6)$$

Following this step, the binomial tail probability of observing $m_{g,\text{obs}}$ from the total of $m_{g,\text{obs}}$ mutations in a gene of interest is:

$$P_{\text{composition}}^{\text{mut}} = P(m_{g,\text{mut}} \geq m_{g,\text{obs}}) = \sum_{j=m_{g,\text{obs}}}^{m_{g,\text{obs}}} \binom{m_{g,\text{obs}}}{j} P_{g,\text{NS}}^j (1 - P_{g,\text{NS}})^{m_{g,\text{obs}} - j} \quad (7)$$

The three test statistics (equations (3, 4 and 7)) rely on three distinct measures for calling a gene significantly mutated: the counts of single-base substitutions, the counts of indels, and the relative counts of non-synonymous to synonymous single-base substitutions. Assuming the independence of these measures, given gene-specific parameters of g_i and L_g , we combine them using Fisher's combined probability test to derive a measure of overall significance for each gene of interest (combined P value). We acknowledge the fact that Fisher's combined probability test is best suited to P values derived from continuous probability distribution functions; however, it has been shown that its application to P values derived from discrete probability distributions results in conservative estimates of P value.

Finally, we apply Bonferroni and Benjamini–Hochberg's correction method to combined P values to control for multiple testing.

Statistical analyses for therapeutic resistance or sensitivity. Statistical models for tumour growth were implemented for each of four mutation profiles that were correlated to resistance or sensitivity to cetuximab treatment. Group A samples had *ERBB2* mutations and/or amplification, *MET* amplification, *EGFR* mutations affecting the ectodomain or kinase domain, *NRAS* mutation, *BRAFV600E*, *FGFR1* amplification, *PDGFRA* mutations affecting the kinase domain and *MAP2K1* K57N. Group B samples had *ERBB2* mutations, *EGFR* mutations affecting the ectodomain or kinase domain, *FGFR1* amplification, *PDGFRA* mutations affecting the kinase domain or *MAP2K1* K57N. Group C samples had amplification of *EGFR* or a mutation or amplification of *IRS2*, while group D samples had amplification or mutation of *IRS2*. As *IRS2* alterations are likely to be predictive of anti-EGFR response in cases without other mechanisms of resistance to EGFR therapy, we excluded two samples that harboured a *MET* amplification or *BRAF* mutation from groups C and D. For each group, Wilcoxon rank sum and Welch's two-sample t -tests were used to evaluate differences in the mean tumour growth between samples with mutation and those without.

Protein structure modelling. The crystal structure of the extracellular domain of the epidermal growth factor receptor in complex with the Fab fragment of cetuximab was retrieved from the Protein Data Bank (accession number 1YY9). This Protein Data Bank entry contains a complex of three biomacromolecules including the extracellular portion of EGFR, cetuximab Fab Light chain, and cetuximab Fab Heavy chain. The EGFR–cetuximab complex was visualized using Deep View Swiss-pdbviewer (SPDBV_4.10_PC).

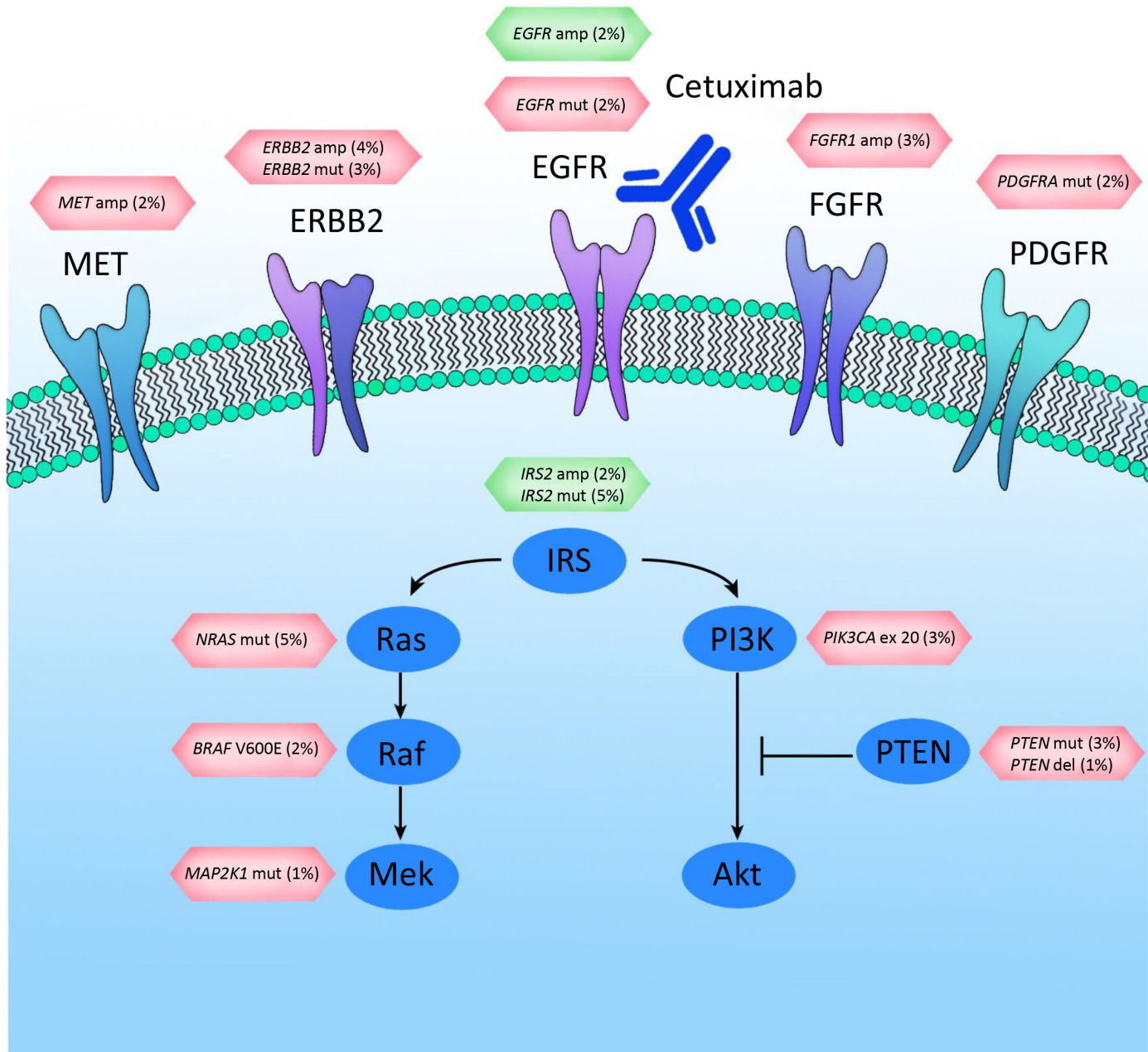
Cell cultures, plasmids, antibodies, and biological assays. NCI-H508 and 293T cells were obtained from ATCC and cultured in RPMI 1640 and Iscove medium, respectively. Cell lines were authenticated for genetic identity by short tandem repeat profiling (Cell ID, Promega) and routinely PCR-tested for mycoplasma contamination (Minerva Biolabs). EGFR G465E and MAP2K1 K57N in the PS100069 lentiviral vectors were custom-cloned by and purchased from OriGene. The MISSION lentiviral pLKO.1-puro shRNA vector targeting *IRS2* (target sequence: GTGAAGATCTGTCTGGCTTTA), as well as the non-targeting control vector, were purchased from Sigma. All vectors were produced by lipofectAMINE 2000 (Life Technologies)-mediated transfection of 293T cells. Primary antibodies included rabbit anti-phospho-Tyr1068-EGFR (ab5644) (Abcam); rabbit anti-EGFR (D38B1), rabbit anti-*IRS2* (L1326), rabbit anti-phospho-Ser473-AKT (D9E), rabbit anti-AKT (11E7), rabbit anti-phospho-Thr202/Tyr204-ERK (D13.14.4E), rabbit anti-ERK (137F5) (Cell Signaling Technology); mouse anti-DDK (4C5) (Origene); and mouse anti-tubulin (DM1A) (Sigma-Aldrich). Proliferative response was assessed with an ATP content assay as an indicator of cellular viability. On day 0, cells were plated at clonal density (20 cells per microlitre) in complete medium. On day 1, serially diluted cetuximab or

vehicle (PBS) was added to the cells. On day 6, cell viability was measured by CellTiter-Glo (Promega) using Victor X4 (PerkinElmer) or GloMax (Promega) microplate luminometers.

Pharmacodynamic analyses. Tumour grafts were embedded in paraffin and subjected to immunoperoxidase staining with rabbit monoclonal antibodies against phospho-S6 (Ser235/236, clone D57.2.2E, Cell Signaling Technology) or phospho-ERK1/2 (Thr202/Tyr204, clone D13.14.4E, Cell Signaling Technology). After incubation with secondary antibodies, immunoreactivities were revealed by incubation in DAB chromogen (Dako). Images were captured with the Leica LAS EZ software using a Leica DM LB microscope. For morphometric quantitation, five fields per section at $\times 40$ magnification from two tumours from two different mice for each treatment modality ($n = 10$) were analysed using ImageJ. Immunoreactivity for phospho-ERK and phospho-S6 was quantified by spectral segmentation of images in two layers: one layer excluded stroma and empty spaces (such as lumens); the second layer measured DAB positivity. The percentage of immunoreactive cells was calculated as DAB positivity divided by total cancer cell area. Software outputs were manually verified by visual inspection of digital images.

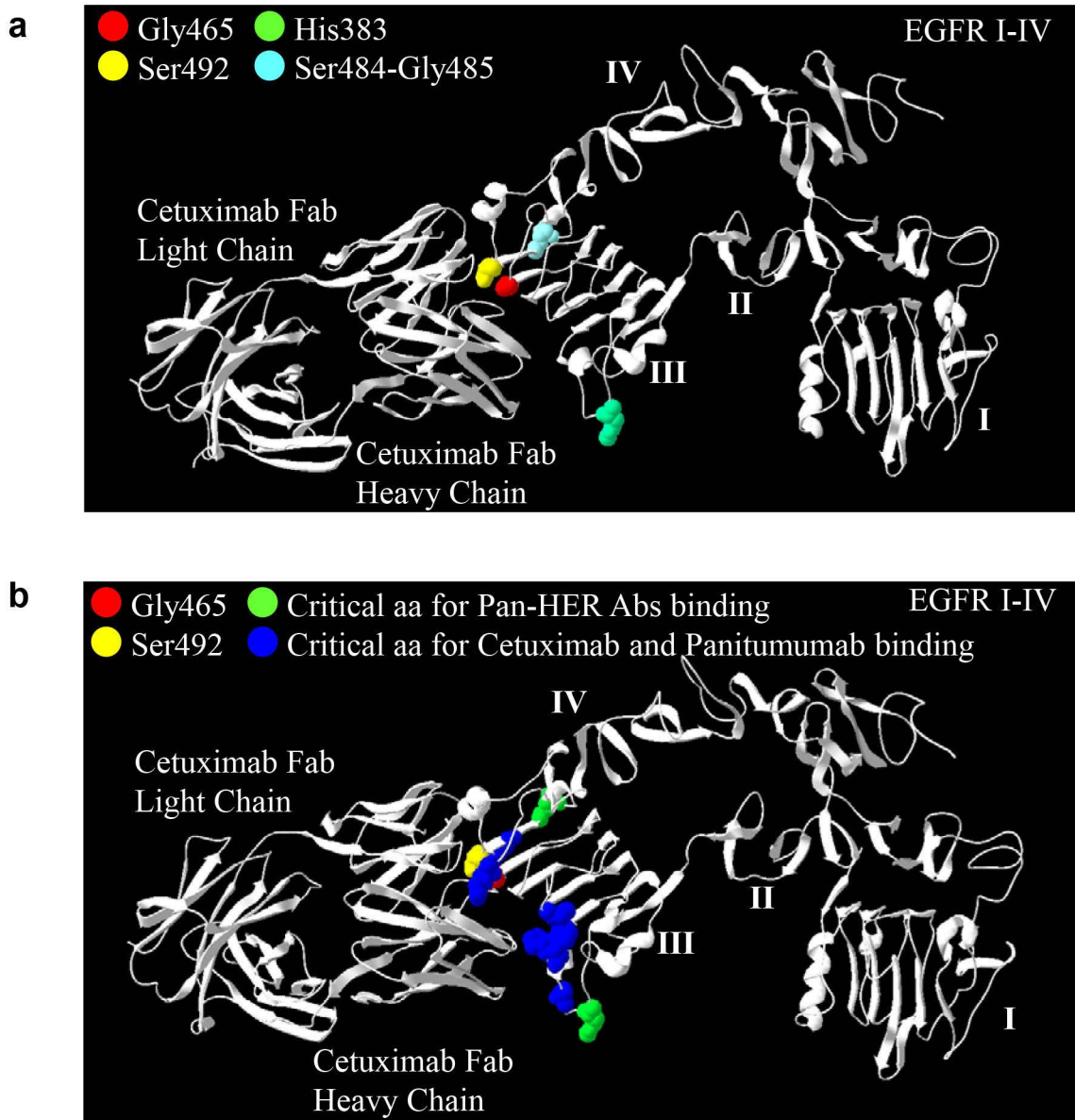
30. Jones, S. et al. Comparative lesion sequencing provides insights into tumor evolution. *Proc. Natl Acad. Sci. USA* **105**, 4283–4288 (2008).

31. Siena, S. et al. Phase II open-label study to assess efficacy and safety of lenalidomide in combination with cetuximab in KRAS-mutant metastatic colorectal cancer. *PLoS One* **8**, e62264 (2013).
32. Galimi, F. et al. Genetic and expression analysis of MET, MACC1, and HGF in metastatic colorectal cancer: response to met inhibition in patient xenografts and pathologic correlations. *Clin. Cancer Res.* **17**, 3146–3156 (2011).
33. Baralis, E., Bertotti, A., Fiori, A. & Grand, A. LAS: a software platform to support oncological data management. *J. Med. Syst.* **36** (Suppl. 1), S81–S90 (2012).
34. Jones, S. et al. Personalized genomic analyses for cancer mutation discovery and interpretation. *Sci. Transl. Med.* **7**, 283ra253 (2015).
35. Needleman, S. B. & Wunsch, C. D. A general method applicable to the search for similarities in the amino acid sequence of two proteins. *J. Mol. Biol.* **48**, 443–453 (1970).
36. Leary, R. J., Cummins, J., Wang, T. L. & Velculescu, V. E. Digital karyotyping. *Nature Protocols* **2**, 1973–1986 (2007).
37. Jiao, Y. et al. Exome sequencing identifies frequent inactivating mutations in BAP1, ARID1A and PBRM1 in intrahepatic cholangiocarcinomas. *Nature Genet.* **45**, 1470–1473 (2013).
38. Sjöblom, T. et al. The consensus coding sequences of human breast and colorectal cancers. *Science* **314**, 268–274 (2006).
39. Kan, Z. et al. Diverse somatic mutation patterns and pathway alterations in human cancers. *Nature* **466**, 869–873 (2010).



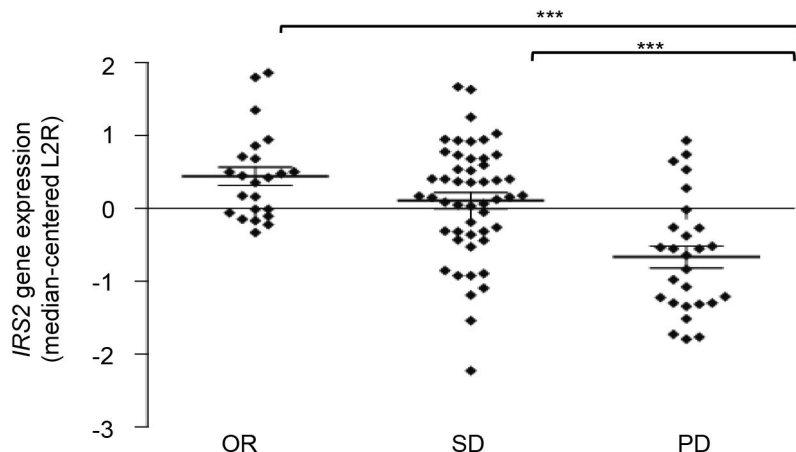
Extended Data Figure 1 | EGFR signalling pathway genes involved in cetuximab resistance or sensitivity. Altered cell-surface receptors or members of RAS or PI3K pathways identified in this study are indicated. Somatic alterations related to resistance or sensitivity are highlighted in red or green boxes, respectively. The percentages indicate the fraction of KRAS wild-type

tumours containing the somatic alterations in the specified genes. For the following genes a subset of alterations are indicated: *PDGFRA* kinase domain mutations; *EGFR* ecto- and kinase domain mutations and amplifications.



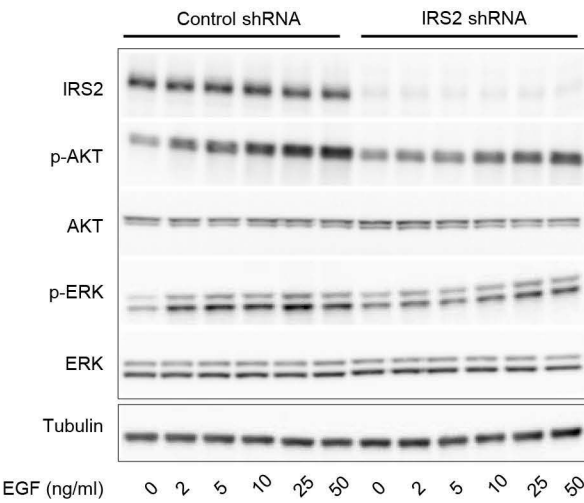
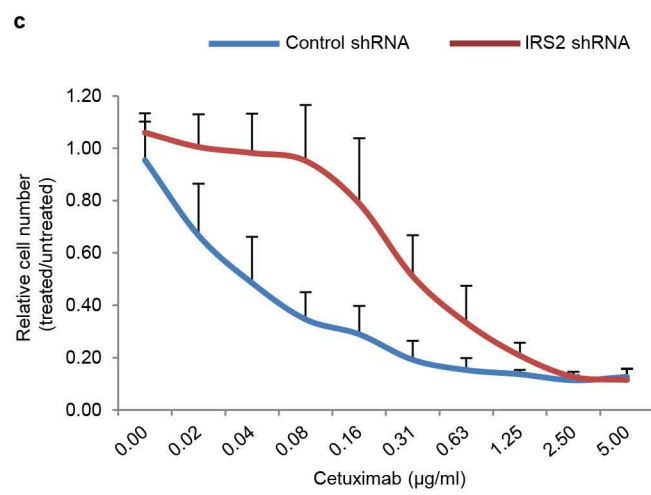
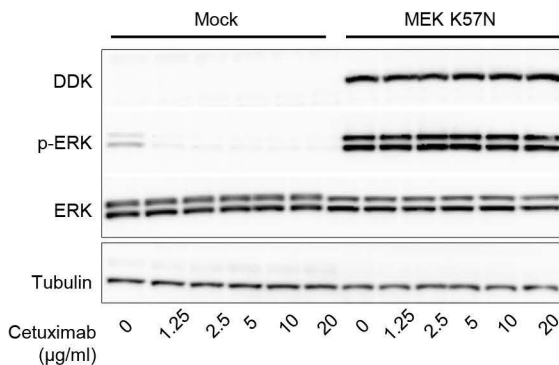
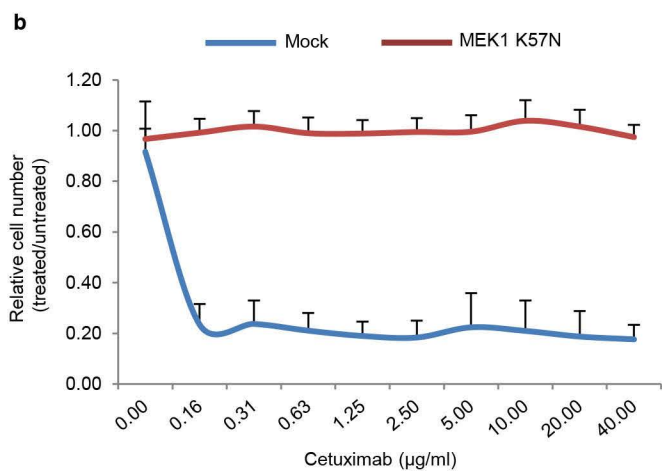
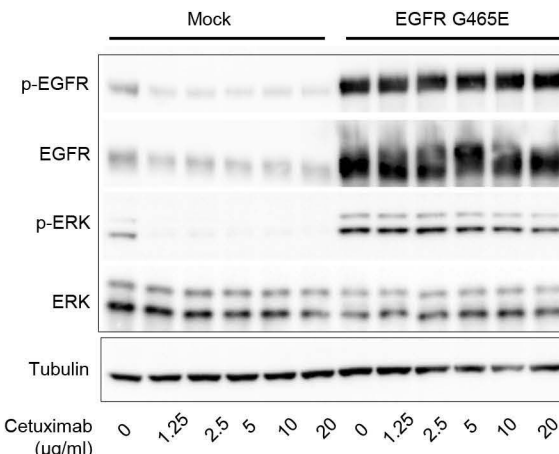
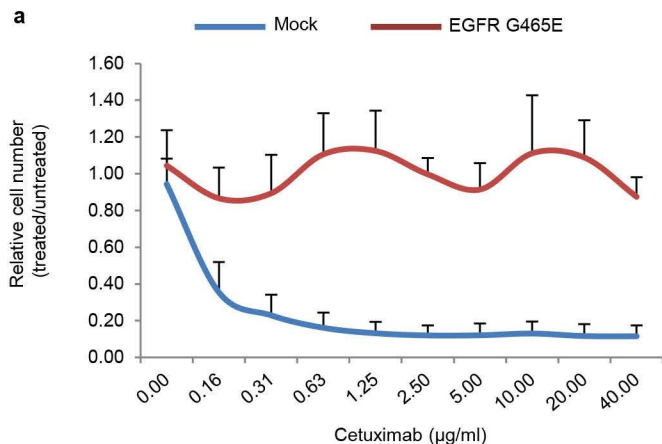
Extended Data Figure 2 | Pan-HER monoclonal antibody mixture binds epitopes different from those recognized by cetuximab. **a,** The H383 (green) and the S484/G485 (light blue) residues in EGFR domain III are critical for the binding of Pan-HER anti-EGFR antibodies 1277 and 1565, respectively²⁸. Antibodies 1277 and 1565 (ref. 28) bind to an epitope distinct from that of cetuximab, which may contribute to the superior tumour growth inhibition in the presence of mutations at residue 465. Mutations identified in this study affecting G465 (red) and the S492 amino acid (yellow) previously reported to confer cetuximab resistance¹¹ are shown for reference. Similarly to mutations

affecting S492, the alterations at 465 that we identified in this study (G465R and G465E) involve changes from a non-polar uncharged side chain to large electrically charged arginine or glutamic acid residues, respectively, and predict resistance to cetuximab. **b,** Critical EGFR amino acids selectively recognized by both cetuximab and panitumumab as determined by phage screening are shown in blue and include P373, K467, P411, K489, D379, F376 (ref. 27). Residue G465 is in close proximity to K467 and other residues that have been shown to influence the binding of both cetuximab and panitumumab²⁷.



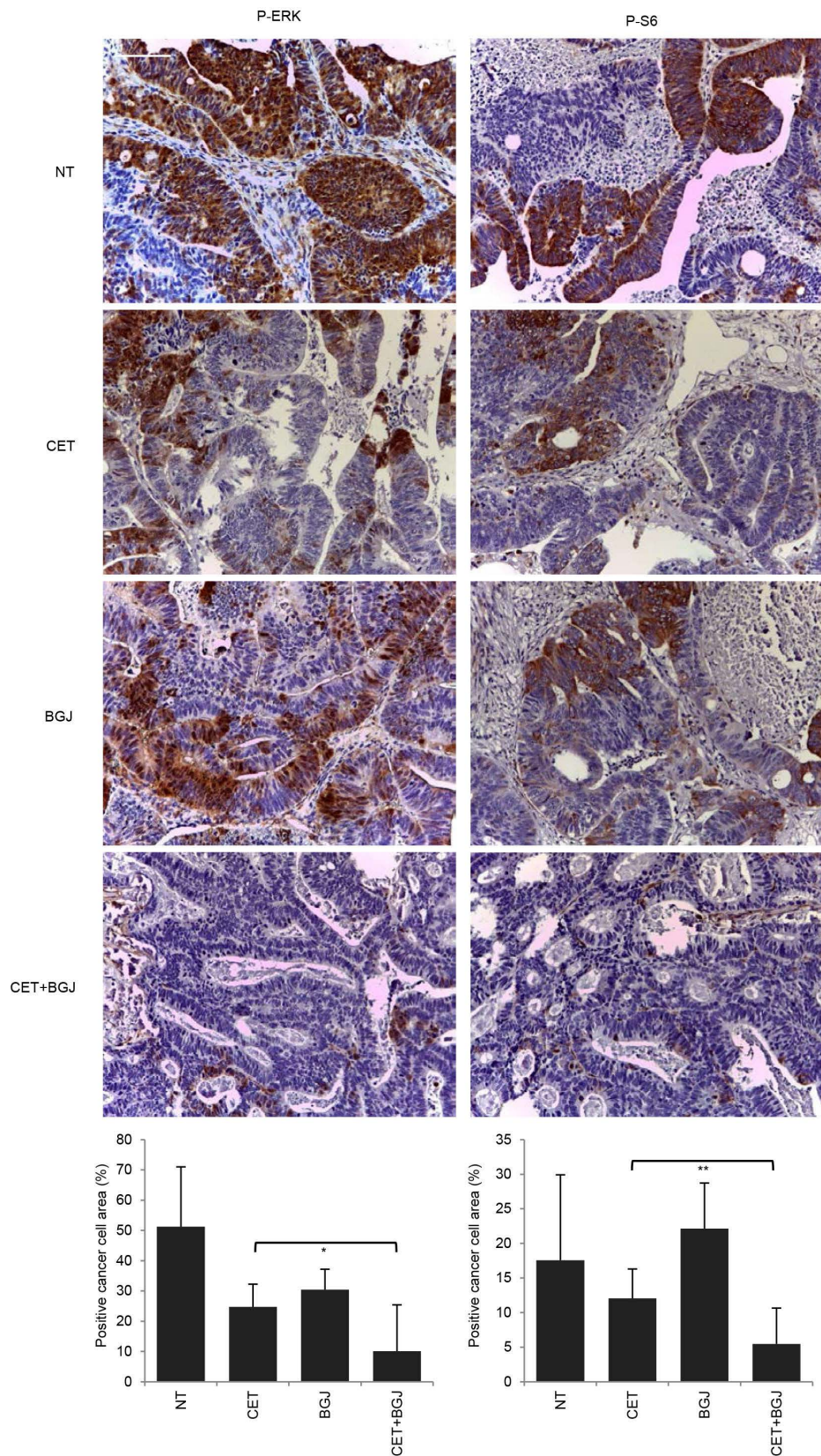
Extended Data Figure 3 | Expression of IRS2 according to response categories in tumour graft models. Results were obtained using Illumina-based oligonucleotide microarrays in 100 tumour grafts that had no mutations in the *KRAS*, *NRAS*, *BRAF*, or *PIK3CA* genes. Response categories are defined

in the main text. OR, objective response; SD, stable disease; PD, progressive disease. $P < 0.001$ for OR compared with PD and SD compared with PD by one-way ANOVA and Bonferroni's multiple comparison test. IRS2 expression values are shown in Supplementary Table 10.



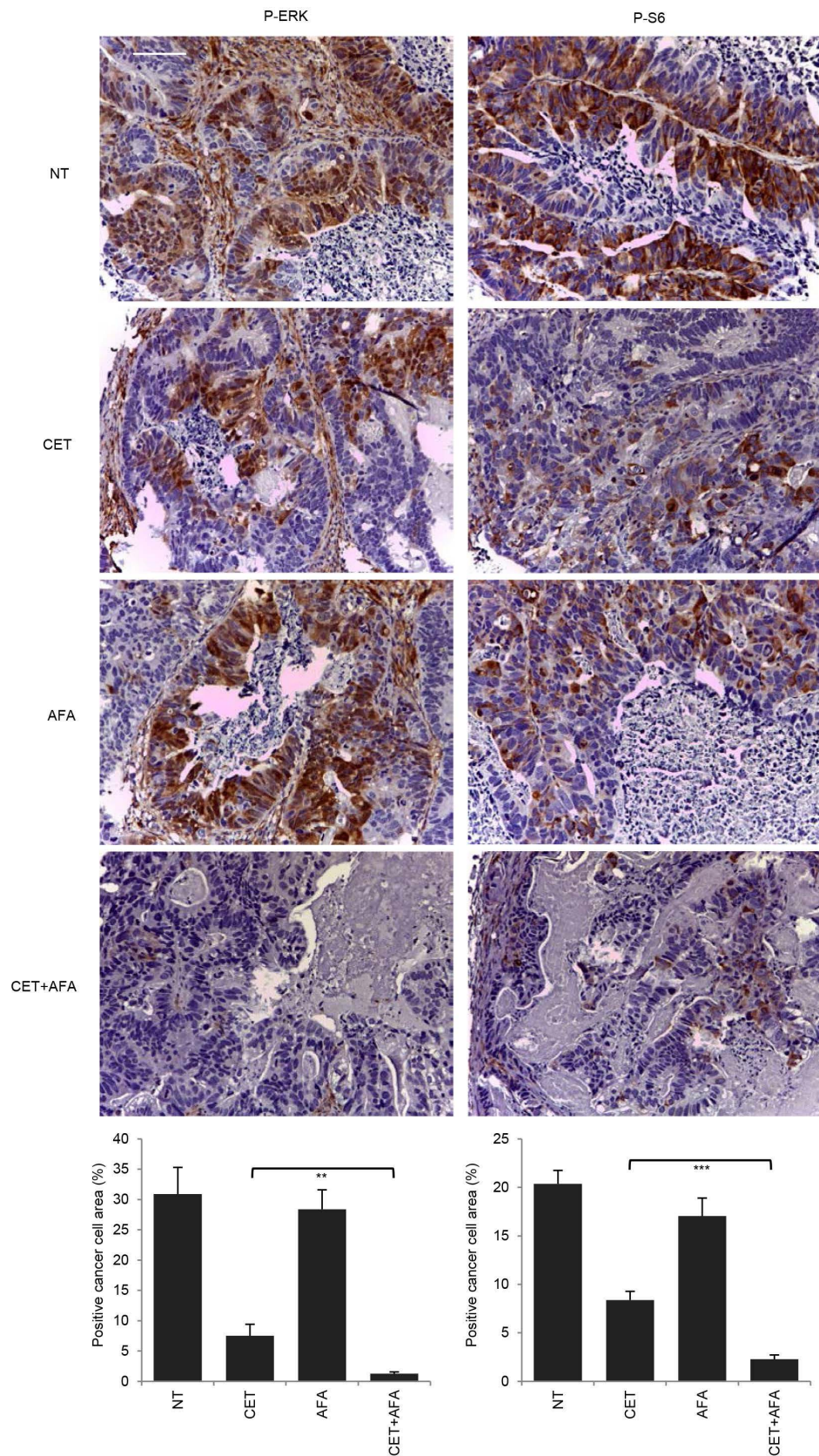
Extended Data Figure 4 | Functional studies of genetic alterations associated with cetuximab response. **a, b**, Ectopic expression of mutations that correlated with resistance to EGFR blockade prevented responsiveness to cetuximab. NCI-H508 cells expressing EGFR G465E (**a**, left) or DDK-tagged MAP2K1 K57N (**b**, left) were refractory to cetuximab in dose-dependent viability assays after 6 days of treatment. Results are the means \pm s.d. of two independent experiments performed in biological triplicates ($n = 6$) for EGFR G465E and three independent experiments performed in biological triplicates ($n = 9$) for MAP2K1 K57N compared with mock vector controls. Biochemical responses of NCI-H508 EGFR G465E (**a**, right) and NCI-H508 MAP2K1 K57N (**b**, right) treated with cetuximab for 24 h were documented by western blot

analyses. **c**, Genetic silencing of IRS2 (IRS2 shRNA) in NCI-H508 cells reduced sensitivity to cetuximab in dose-dependent viability assays (left). Results are the means \pm s.d. of two independent experiments performed in biological triplicates ($n = 6$). In biochemical studies using western blot analyses (right), IRS2 knockdown attenuated EGF-dependent activation of AKT (P-AKT) and ERK (P-ERK). Cells were treated for 10 min with the indicated concentrations of EGF. Tubulin was used as a loading control. Western blots for total EGFR, ERK, and AKT proteins were run with the same lysates as those used for anti-phosphoprotein detection but on different gels. All western blots are representative of two independent experiments.



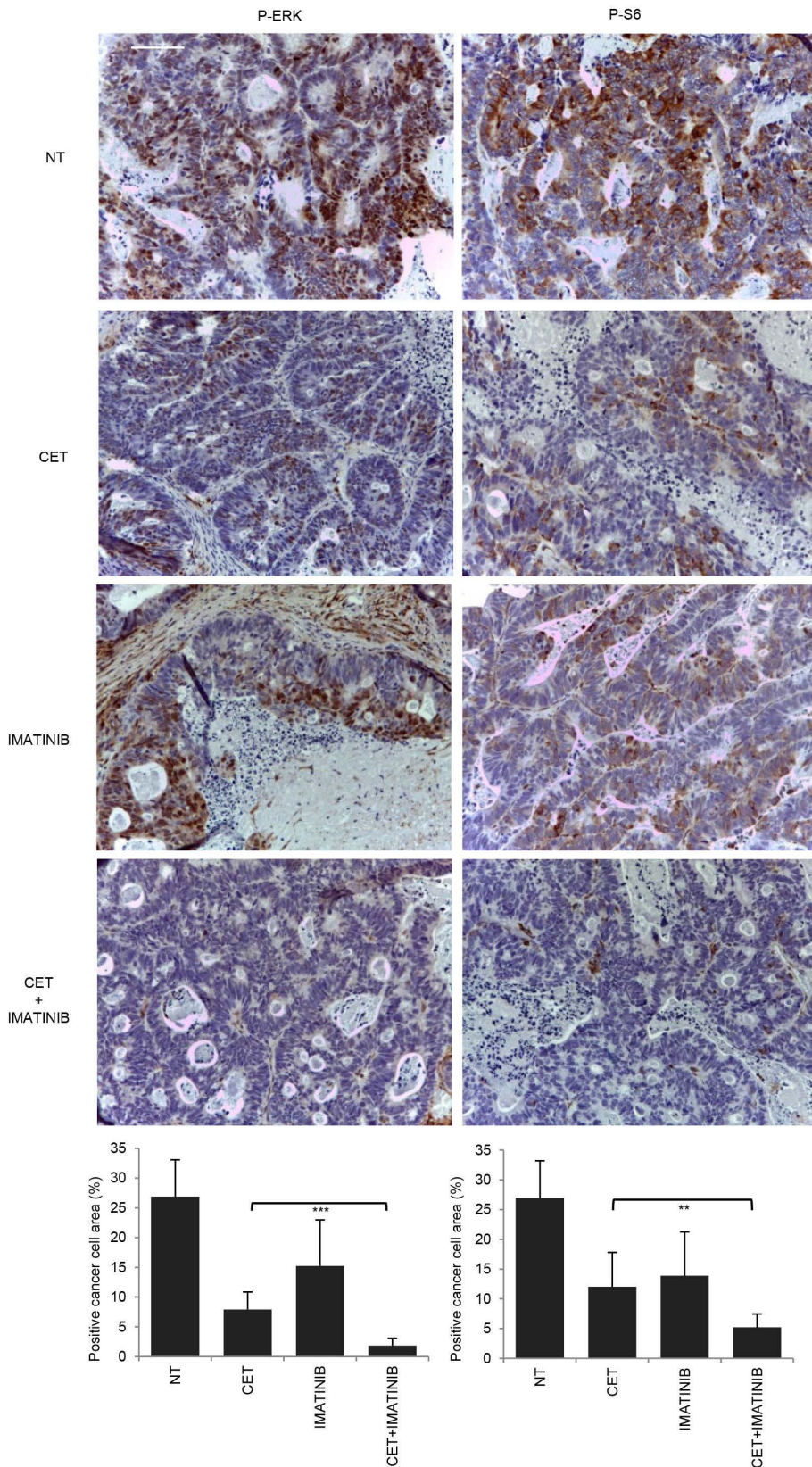
Extended Data Figure 5 | Signalling consequences of FGFR inhibition in FGFR1-amplified CRC477. Immunohistochemistry with the indicated antibodies and morphometric quantitations of representative tumours at the end of treatment. Results are the means \pm s.d. of five fields ($\times 40$) from two

tumours for each experimental point ($n = 10$). Scale bar, 300 μ m. P-ERK, phospho-ERK; P-S6, phospho-S6. NT, not treated (vehicle); CET, cetuximab; BGJ, BGJ398. * $P < 0.05$; ** $P < 0.01$ by two-tailed Student's *t*-test.



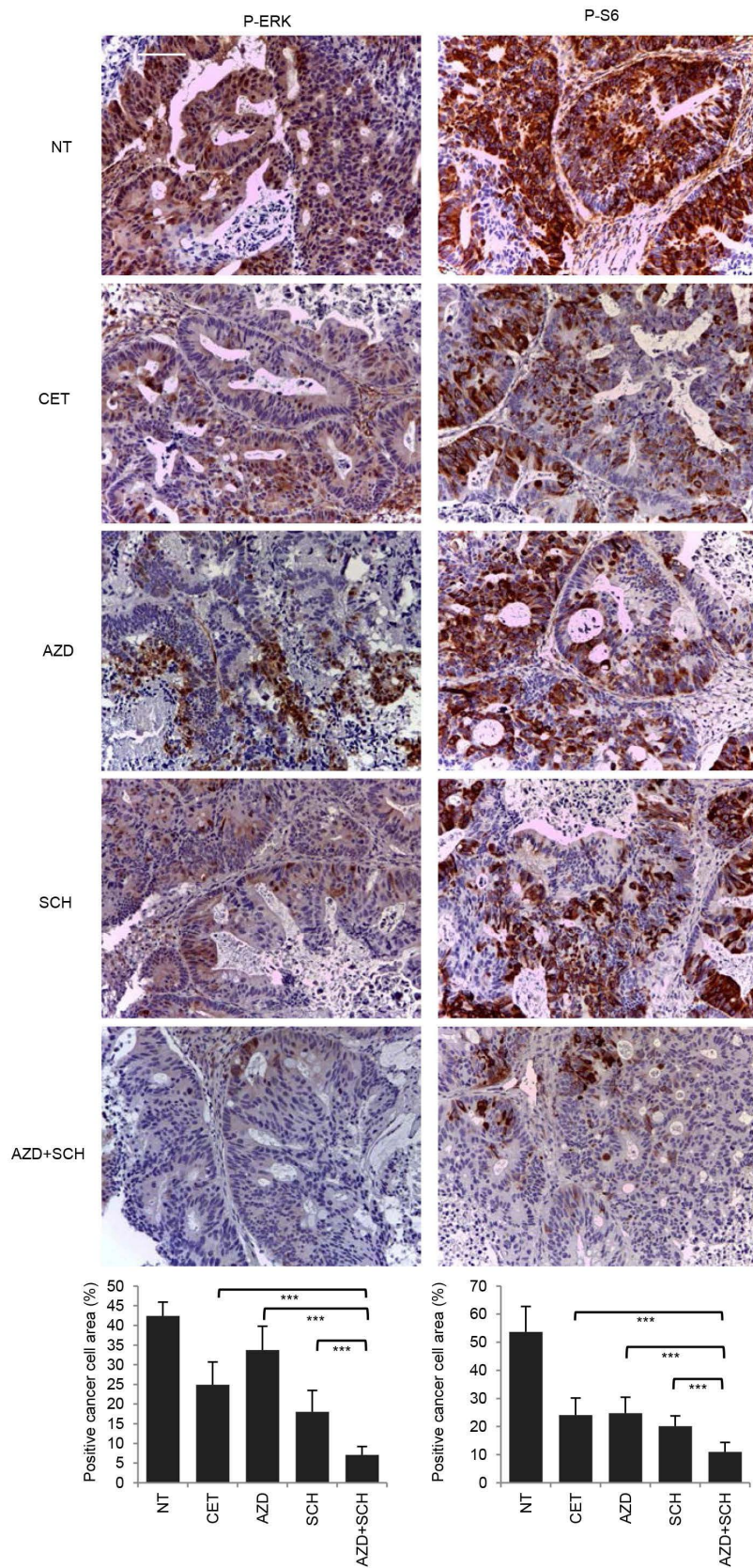
Extended Data Figure 6 | Signalling consequences of EGFR inhibition in EGFR mutant (V843I) CRC334. Immunohistochemistry with the indicated antibodies and morphometric quantitations of representative tumours at the

end of treatment. Results are the means \pm s.d. of five fields ($\times 40$) from two tumours for each experimental point ($n = 10$). Scale bar, 300 μm . AFA, afatinib. ** $P < 0.01$; *** $P < 0.001$ by two-tailed Student's t -test.



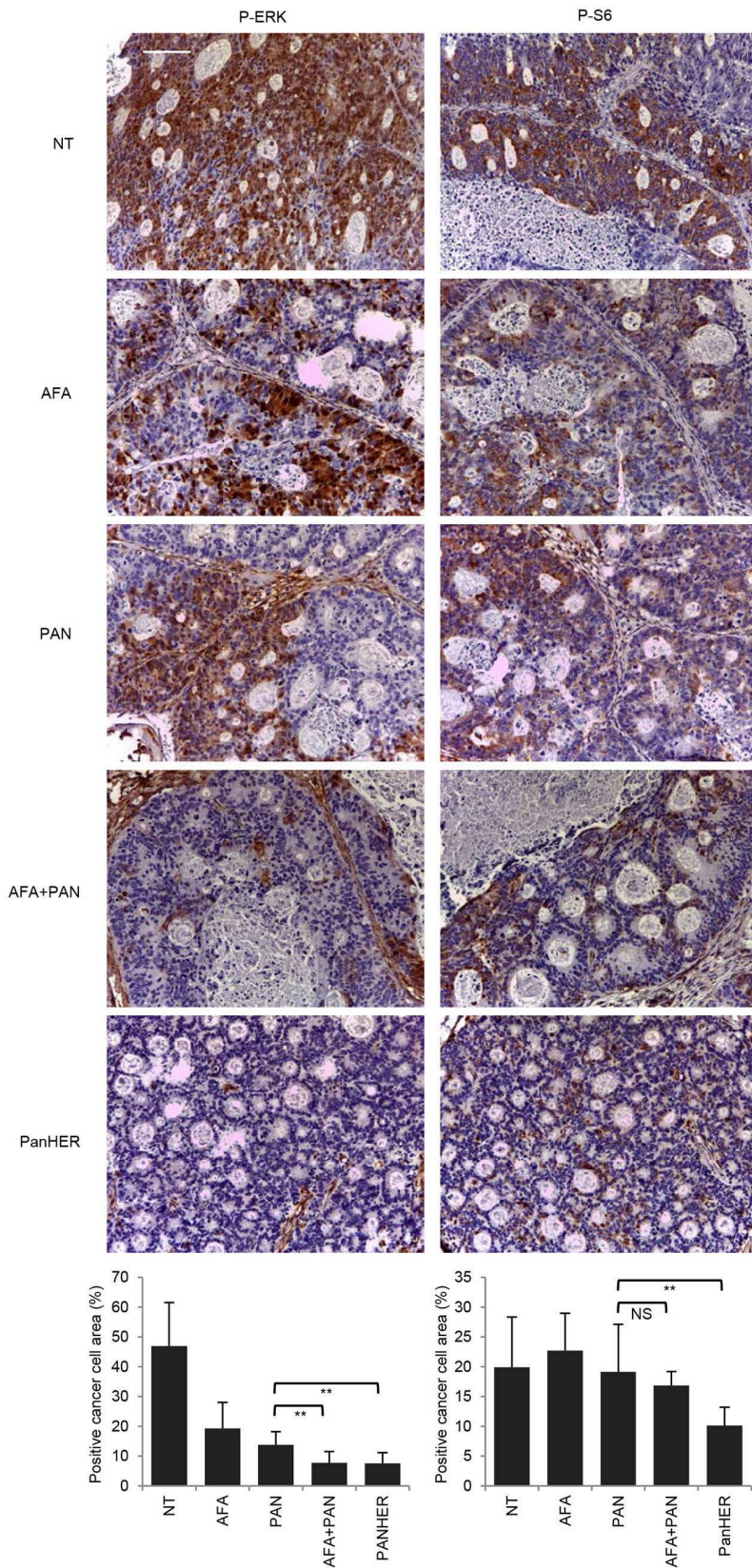
Extended Data Figure 7 | Signalling consequences of PDGFR inhibition in PDGFRA mutant (R981H) CRC525. Immunohistochemistry with the indicated antibodies and morphometric quantitations of representative tumours after acute treatment (4 h after imatinib and 24 h after cetuximab

administration). Results are the means \pm s.d. of five fields ($\times 40$) from two tumours for each experimental point ($n = 10$). Scale bar, 300 μm . ** $P < 0.01$ by two-tailed Student's t -test.



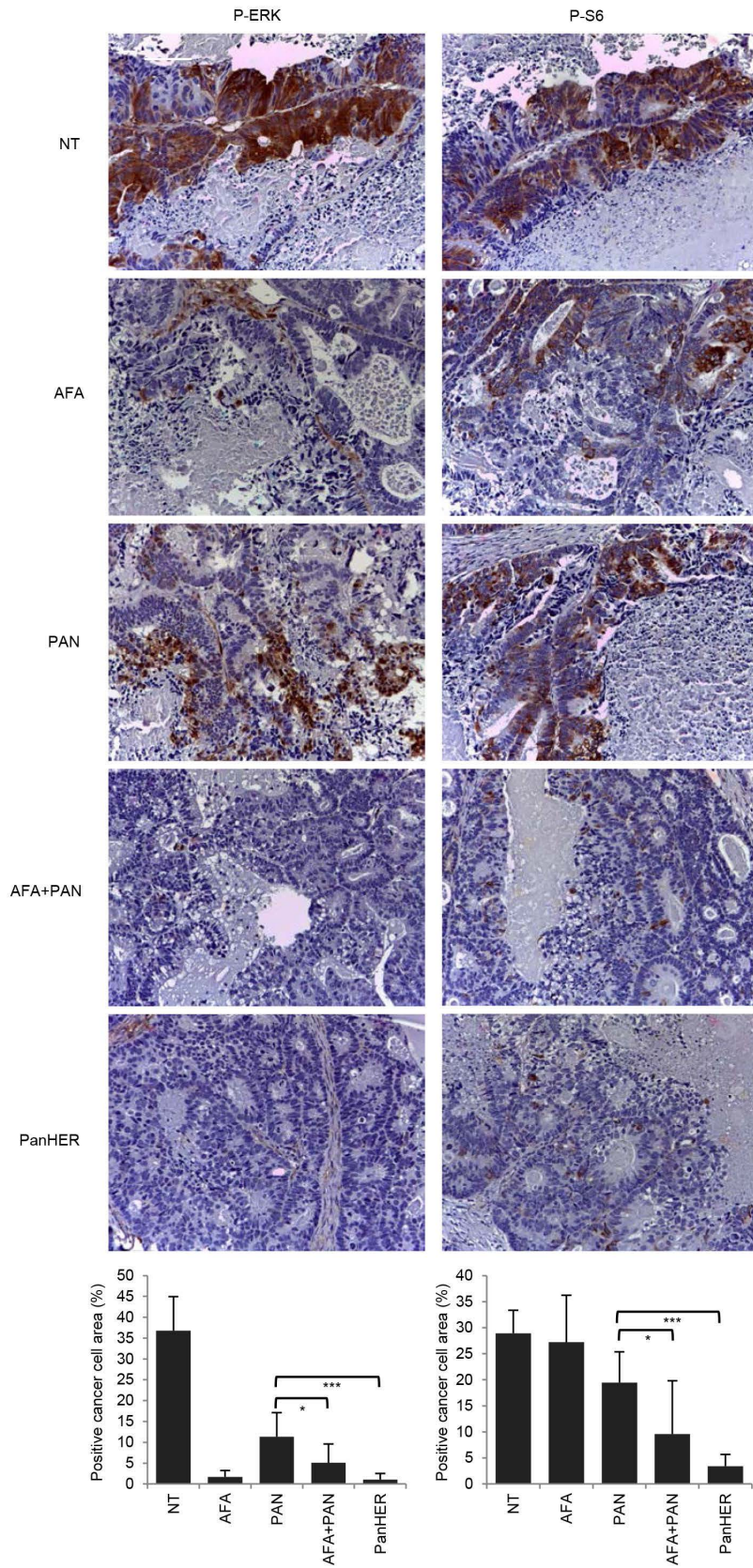
Extended Data Figure 8 | Signalling consequences of MEK1 inhibition in MAP2K1 mutant (K57KN) CRC343. Immunohistochemistry with the indicated antibodies and morphometric quantitations of representative tumours at the end of treatment. Results are the means \pm s.d. of five

fields ($\times 40$) from two tumours for each experimental point ($n = 10$). Scale bar, 300 μm . AZD, AZD6244; SCH, SCH772984. *** $P < 0.001$ by two-tailed Student's *t*-test.



Extended Data Figure 9 | Signalling consequences of EGFR inhibition in EGFR mutant (G465E) CRC104. Immunohistochemistry with the indicated antibodies and morphometric quantitations of representative tumours at the end of treatment. Results are the means \pm s.d. of five fields

($\times 40$) from two tumours for each experimental point ($n = 10$). Scale bar, 300 μm . PAN, panitumumab. NS, not significant; ** $P < 0.01$ by two-tailed Student's *t*-test.



Extended Data Figure 10 | Signalling consequences of EGFR inhibition in EGFR mutant (G465R) CRC177. Immunohistochemistry with the indicated antibodies and morphometric quantitations of representative tumours at the

end of treatment. Results are the means \pm s.d. of five fields ($\times 40$) from two tumours for each experimental point ($n = 10$). Scale bar, 300 μm . * $P < 0.05$; *** $P < 0.001$ by two-tailed Student's t -test.